Breather–phonon resonances in finite-size lattices: 'phantom breathers'?

2002 J. Phys. A: Math. Gen. 35 4999

(http://iopscience.iop.org/0305-4470/35/24/303)

INSTITUTE OF PHYSICS PUBLISHING JOURNAL OF PHYSICS A: MATHEMATICAL AND GENERAL

J. Phys. A: Math. Gen. **35** (2002) 4999–5021 PII: S0305-4470(02)34583-9

Breather–phonon resonances in finite-size lattices: 'phantom breathers'?

Anna Maria Morgante[1], **Magnus Johansson**[2], **Serge Aubry**[1] **and Georgios Kopidakis**[3]

[1] Laboratoire Léon Brillouin (CEA-CNRS), CEA Saclay, F-91191 Gif-sur-Yvette Cedex, France
[2] Department of Physics and Measurement Technology, Linköping University, S-581 83 Linköping, Sweden
[3] Department of Physics, University of Crete, PO Box 2208, GR-71003 Heraklion, Crete, Greece

E-mail: mjn@ifm.liu.se

Received 28 February 2002, in final form 26 April 2002
Published 7 June 2002
Online at stacks.iop.org/JPhysA/35/4999

Abstract

We investigate the resonance mechanisms for discrete breathers in finite-size Klein–Gordon lattices, when some harmonic of the breather frequency enters the linear phonon band. For soft on-site potentials, the second-harmonic resonances typically result in the appearance of solutions with non-zero tails, phonobreathers. However, these tails may be very weak, and for small systems where the phonon frequencies are sparsely distributed, we identify 'phantom breathers' as being practically localized solutions, existing with frequencies in-between the phonon frequencies. For particular parameter values the tails completely vanish, and the phantom breathers decay exponentially over the whole system. We also describe briefly a first-harmonic resonance with a constant-amplitude wave and the generation of phonobreathers for hard potentials.

PACS numbers: 63.20.Ry, 05.45.−a, 05.50.+q, 45.05.+x

1. Introduction

Discrete breathers, or intrinsically localized modes, are exact, time-periodic and spatially localized, solutions of nonlinear discrete systems. They are universal in the sense that their existence does not require any integrability properties of the mathematical model, and they may exist in finite as well as infinite systems, in arbitrary dimension and in the absence as well as presence of disorder. See, e.g., [1, 2] for general reviews and [3, 4] for more recent developments. A discrete breather belongs generically to a one-parameter family of exact solutions to some given model, where the parameter chosen can be, e.g., its frequency, action or energy. In addition, these breather families are generically robust, surviving for

small perturbations of the model, so that they can also be continued as a function of some model parameter. Moreover, discrete breathers are often (but not always) linearly stable, and even though this does not imply their strict stability for all times, at least any small initial perturbation will grow slower than exponentially with time, so that a slightly perturbed breather typically will have a very long lifetime. Obviously, the lifetime of the unperturbed breather will be infinite as it is an exact solution.

The fact that the energy of a time-periodic discrete breather can remain localized forever without being dispersed to its surroundings basically rests on two properties of the system: nonlinearity and spatial discreteness. To avoid energy dispersion of a localized anharmonic oscillatory mode into small amplitude vibrations, generically one should avoid resonances between harmonics of the mode frequency and the frequencies of the linear oscillation modes, 'phonons'. Denoting the breather frequency with ω_b and the phonon frequencies with $\omega_0(\boldsymbol{q})$, this *non-resonance condition* becomes

$$m\omega_b \neq \omega_0(\boldsymbol{q}) \qquad \forall m \text{ integer.} \tag{1}$$

The role of the nonlinearity is then to provide a nontrivial dependence of the mode frequency on its amplitude (or, equivalently, on its action), so that the frequency of a finite-amplitude oscillation does not remain fixed at its linear value. Furthermore, the role of the discreteness is to provide an upper bound to the linear phonon spectrum (and possibly gaps within it), and thus renders possible the scenario where not only the fundamental mode frequency but also all its higher harmonics lie outside (or in gaps within) the linear spectrum. These intuitive physical arguments for the existence of localized oscillatory modes as exact solutions have been turned into several rigorous existence proofs [1, 5–11], and spatial exponential decay for the oscillation amplitudes has been proved under quite general conditions [5, 12].

Thus, we generically do not expect to find strictly (e.g. exponentially) localized breather solutions when the non-resonance condition (1) is violated. A typical scenario appearing in simple models with gapless linear spectra when continuing (e.g. numerically) a breather versus its frequency (or versus some model parameter) towards regimes of linear resonance was described in [13]. When the fundamental breather frequency ω_b approaches the linear phonon band, the size of the breather generally diverges and its maximum amplitude goes to zero, and the breather approaches a linear band edge phonon [14]. On the other hand, when a higher breather harmonic ($m > 1$ in (1)) approaches the phonon band while the fundamental harmonic remains outside, a new type of solution smoothly appears from the continuation of the breather. This solution, which has been termed alternatively *phonobreather* [1, 13] or *nanopteron* [2, 15] consists of a (nonlinear) superposition of a localized breather oscillating at the fundamental frequency and an extended band edge standing-wave phonon tail oscillating at the higher harmonic. In more complicated models, e.g. with a nonmonotonic linear dispersion relation $\omega_0(\boldsymbol{q})$ [16], phonobreathers may also result from resonances at the fundamental breather frequency ω_b.

As has been remarked already in [13], if the numerical continuation of a localized breather with a higher harmonic entering the linear phonon band is performed 'with bigger steps and less care', other phonobreather-like solutions might be found but with 'defects' in the phonon tail. It was also remarked in [13] that for small finite systems even apparently localized breather-like solutions with negligible tails could be found, as the large separation of the discrete phonon frequencies $\omega_0(\boldsymbol{q})$ in a small system could allow for windows of non-resonance inside the band. We will here introduce the term *phantom breather* for this type of practically localized solution, possibly existing in frequency intervals which should be forbidden for localized solutions in infinite systems. It is the purpose of the present paper to describe, by a systematic numerical analysis of a simple model system, a typical bifurcation scenario for

the penetration of a breather harmonic into the linear phonon band for finite-size systems, and to provide a working definition of 'phantom breathers' in terms of their properties. For generic values of the model parameters, the phantom breathers are found to have small but non-zero tails with oscillation patterns corresponding to nearby phonon modes; however, for particular parameter values the contributions from modes having the same pattern but opposite phases may cancel each other and yield phantom breathers which are exponentially localized over the whole system. It should be noted that a related problem was considered in [17, 18] where the continuation of a breather inside the linear band was investigated for a *disordered* system. However, even though as we will see there are many similarities in the bifurcation scenarios, the problems are fundamentally different since for the disordered system also the linear modes are exponentially (Anderson) localized, and as a consequence strictly localized intraband breathers could be found generically also for infinite systems in the latter case [18].

The outline of this paper is as follows. In section 2 we present the model system, which we take to be a one-dimensional Klein–Gordon (KG) lattice, and briefly describe the ideas developed in [1, 5] to classify breather-type solutions by using an anticontinuous limit. In section 3 we apply numerical continuation techniques to analyse a number of different aspects of breather–phonon resonances in finite systems. The main emphasis is put on the case with a soft potential, which we choose to be of Morse type, and we describe the smooth continuation of breathers into phonobreathers, as well as the occurrence of 'phantom breathers' and the mechanism leading to the vanishing of their tails at special parameter values. We also describe briefly a first-harmonic resonance with a constant-amplitude ($q = 0$) wave, and show an example of the generation of phonobreathers in a hard on-site potential, which is taken to be quartic. Section 4 concludes the paper, and in appendix A we illustrate how the technique of band analysis [1] can be used to describe additional aspects of the breather–phonobreather transition. Some further considerations of the bifurcation scenarios are presented in [19].

2. The Klein–Gordon lattice: continuation of breathers and multibreathers from an anticontinuous limit

The model system that we will consider consists of a one-dimensional chain of N particles of unit mass, oscillating in an anharmonic on-site potential $V(u)$ and coupled by a harmonic nearest-neighbour coupling C_{K}. Denoting by $u_n(t)$ the displacement of the particle n, the Hamiltonian is written as

$$H = \sum_{n=1}^{N} \left[\frac{1}{2}\dot{u}_n^2 + V(u_n) + \frac{1}{2}C_{\mathrm{K}}(u_{n+1} - u_n)^2 \right]. \tag{2}$$

We will consider closed chains and impose the periodic boundary conditions $u_0 = u_N$, $u_{N+1} = u_1$. The equations of motion then take the form of a discrete nonlinear Klein–Gordon equation,

$$\ddot{u}_n + V'(u_n) - C_{\mathrm{K}}(u_{n+1} + u_{n-1} - 2u_n) = 0. \tag{3}$$

We distinguish between soft and hard on-site potentials $V(u)$, for which the oscillation frequency decreases and increases, respectively with increasing amplitude of the oscillation (or, equivalently, with increasing action). In this paper we mainly consider the soft case, and as a concrete example we choose the Morse potential,

$$V(u) = \tfrac{1}{2}(\mathrm{e}^{-u} - 1)^2. \tag{4}$$

As an example of a hard potential, we choose the quartic potential,

$$V(u) = \frac{u^2}{2} + \frac{u^4}{4}. \tag{5}$$

In both cases we have normalized to have $V''(0) = 1$, i.e. the oscillation frequency is unity for small-amplitude (harmonic) oscillations in the absence of coupling.

For a given solution $\{u_n(t)\}$ to (3), the dynamics of a small-amplitude perturbation $\{\epsilon_n(t)\}$ can be approximated by the linearization of (3) around $\{u_n(t)\}$, which yields the Hill equations

$$\ddot{\epsilon}_n + V''(u_n(t))\epsilon_n(t) - C_K(\epsilon_{n+1}(t) + \epsilon_{n-1}(t) - 2\epsilon_n(t)) = 0. \tag{6}$$

In particular, for $u_n \equiv 0$, the standard harmonic plane waves with wave vector q and frequency $\omega_0(q)$ are obtained,

$$\epsilon_n(t) = \epsilon \cos(qn - \omega_0(q)t) \tag{7}$$

describing the spectrum of the linear (phonon) oscillation frequencies through the dispersion relation

$$\omega_0^2(q) = 1 + 4C_K \sin^2 \frac{q}{2}. \tag{8}$$

Thus, the linear spectrum is bounded to the frequency interval $[1, \sqrt{1+4C_K}]$.

Localized anharmonic solutions (discrete breathers) with frequency ω_b fulfilling the non-resonance condition (1) are then generally found with frequencies below the linear band, i.e. $\omega_b < 1$, for soft potentials, and above the linear band, i.e. $\omega_b > \sqrt{1+4C_K}$, for hard potentials. A convenient way to identify breather-type solutions is to consider the so-called *anticontinuous* [1, 5] limit of uncoupled oscillators, i.e. to let $C_K \to 0$. Restricting to time-reversible solutions fulfilling $u_n(t) = u_n(-t)$, a general time-periodic solution with period $T_b = 2\pi/\omega_b$ can, at this limit, be described by specifying the particular oscillatory state of the nth particle through a *code* σ_n defined as [1]

- $\sigma_n = 0$: for oscillator n at rest;
- $\sigma_n = +p$: for oscillator n oscillating at frequency $p\omega_b$ in phase with some chosen reference solution;
- $\sigma_n = -p$: for oscillator n oscillating at frequency $p\omega_b$ in antiphase with the reference solution;

where p is an arbitrary positive integer. Then, assuming the non-resonance condition (1) to be fulfilled, these solutions are proved [1, 5] to be *uniquely* continuable up to some finite value of the coupling C_K, and thus each anticontinuous coding sequence $\{\sigma_n\}$ identifies uniquely a particular time-periodic solution with period T_b. We define the *simple breather* to be the solution with code [. . . 00000100000 . . .], i.e. the solution for which one single site oscillates at frequency ω_b while all other sites are at rest at the anticontinuous limit. All other time-periodic solutions that can be obtained by unique continuation from the anticontinuous limit, corresponding to more than one oscillating site at this limit, are called *multibreathers* [1]. In general, for infinite systems, we will use the term multibreather for solutions with finitely as well as infinitely many sites with $\sigma_n \neq 0$. In the first case, the solution will still be localized, while in the second case the solution is obviously extended.

A particularly interesting class of multibreather solutions can be constructed by the periodic (or, for an infinite system, possibly quasiperiodic) repetition of the codes $+p, 0, -p$ obtained by writing $\sigma_n = p\chi(qn + \phi)$, where the function $\chi(x)$ is 2π-periodic and, in the case of a soft potential, defined for $x \in [-\pi, \pi]$ as [20, 21]

$$\chi(x) = \begin{cases} +1 & \text{for} \quad (\pi - q)/2 \leqslant x \leqslant (\pi + q)/2 \\ -1 & \text{for} \quad -(\pi + q)/2 \leqslant x \leqslant -(\pi - q)/2 \\ 0 & \text{elsewhere.} \end{cases} \tag{9}$$

As long as the amplitude u_n and coupling C_K remain small, these solutions were found [20, 21] to continue smoothly to harmonic standing-wave phonons of the form

$u_n(t) \sim \sin(qn+\phi)\cos(p\omega_b t)$ when their frequency $p\omega_b$ approaches the linear oscillation frequency $\omega_0(q)$ given by (8). Thus, we can identify these solutions as the *nonlinear standing-wave phonons*. For a hard potential, the transformation $\sigma_n \to (-1)^n\sigma_n$ of the above generated coding sequence yields nonlinear standing-wave phonons with wave vector $\pi - q$ with similar properties [21].

Another type of multibreather solution, which will be of particular interest in this work, is the phonobreather, which can be constructed by superposing the anticontinuous coding sequences for a standing-wave phonon and a simple breather. For a soft potential, in order to yield a small-amplitude tail the phonon part should oscillate at a higher harmonic of the fundamental breather frequency ω_b. So, for example, phonobreathers formed with the phonon wave vector $q = \pi$ will have codes of type $[\cdots+2-2+2-2+2\pm1+2-2+2-2+2\cdots]$, $[\cdots+2-2+2\pm1-2+2-2\cdots]$ (symmetric and antisymmetric with respect to the central breather site, respectively) or $[\cdots+3-3+3-3+3\pm1+3-3+3-3+3\cdots]$ etc. By contrast, for a hard potential, to obtain a small-amplitude tail the breather frequency should be a multiple of the phonon frequency so, for example, the phonobreathers formed with the phonon wave vector $q = 0$ will have codes of type $[\cdots+1+1+1+1+1\pm2+1+1+1+1+1\cdots]$, $[\cdots+1+1+1+1+1\pm3+1+1+1+1+1\cdots]$ (and their antisymmetric counterparts) etc.

3. Breather–phonon resonances analysed through numerical continuation

The numerical continuation of an arbitrary multibreather solution, defined by its anticontinuous coding sequence σ_n, versus, e.g., the coupling C_K and/or the frequency $\omega_b = 2\pi/T_b$ can be performed using standard iterative techniques (see, e.g., [13]), where for each new parameter value a numerically exact solution is calculated from a trial solution obtained in the previous iteration step. In each iteration step, a modified Newton algorithm, described in detail in [17], is used to find solutions $\{u_n(t)\}$ which are time reversible and time periodic with the desired period T_b to an accuracy which is only limited by the computer precision. When the coding sequence of the solution has a definite symmetry, the numerical continuation is facilitated by explicitly imposing a symmetry condition in the Newton scheme to restrict the space of solutions to those compatible with this symmetry [21]. Once the solution $\{u_n(t)\}$ is determined, we obtain also its linear stability properties from the numerical integration of the Hill equations (6) over the period T_b. Relating the $2N$-dimensional vectors $(\{\epsilon_n(0)\}, \{\dot\epsilon_n(0)\})$ and $(\{\epsilon_n(T_b)\}, \{\dot\epsilon_n(T_b)\})$ defines a symplectic $2N \times 2N$ Floquet matrix $\mathbf{F_0}(\{u_n\})$,

$$\begin{pmatrix}\{\epsilon_n(T_b)\}\\ \{\dot\epsilon_n(T_b)\}\end{pmatrix} = \mathbf{F_0}\begin{pmatrix}\{\epsilon_n(0)\}\\ \{\dot\epsilon_n(0)\}\end{pmatrix} \tag{10}$$

and the solution $\{u_n(t)\}$ is linearly stable if and only if all eigenvalues $\Lambda = r\,e^{i\theta}$ of $\mathbf{F_0}$ lie on the unit circle.

3.1. The Morse potential

Considering now the soft Morse potential (4), we will continue numerically a simple breather defined at the anticontinuous limit $C_K = 0$ with frequency $\omega_b < 1$ and code $[\ldots00001000\ldots]$, and our particular interest lies in describing the regime where the second harmonic $2\omega_b$ enters the phonon band defined by (8). This continuation, which will be performed by varying one of the parameters (ω_b, C_K), is schematically illustrated in figure 1. As shown in figure 1(*b*), it is often more convenient to visualize the penetration of higher harmonics $m\omega_b$ into the phonon band $1 < \omega_b < \sqrt{1+4C_K}$ as a penetration of the fundamental frequency ω_b into one of the bands $\frac{1}{m} < \omega_b < \frac{1}{m}\sqrt{1+4C_K}$. Typically, we will follow two different kinds of path illustrated

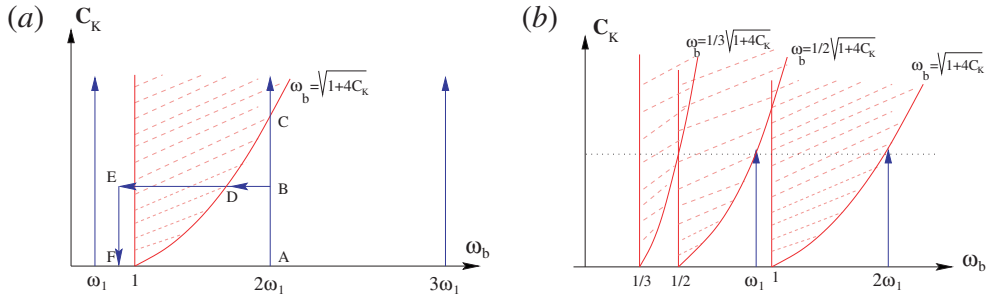

Figure 1. Schematic picture in the (ω_b, C_K)-plane of the penetration of a breather harmonic into the linear phonon band. (*a*) Direct representation with the band $1 < \omega_b < \sqrt{1+4C_K}$ and the breather harmonics $m\omega_1$ ($m = 1, 2, 3, \ldots$); (*b*) alternative representation with a sequence of bands $\frac{1}{m} < \omega_b < \frac{1}{m}\sqrt{1+4C_K}$ and only the fundamental frequency $\omega_b = \omega_1$.

by the lines A-B-D-E-F and A-B-C in figure 1(*a*), respectively. In the first case, we can study the behaviour as the second breather harmonic traverses the whole band by decreasing ω_b for fixed C_K and then for fixed $\omega_b < 0.5$, a continuation back to the anticontinuous limit by decreasing C_K can be performed to check the code of the solution after the crossing of the phonon band (as we shall see, this code is generally different from the original code). With the second path, increasing C_K at constant ω_b, in addition to analysing the entrance into the band we can also obtain the behaviour of the solution at large couplings, which typically also implies large oscillation amplitudes.

3.1.1. Smooth continuation into a phonobreather. A typical scenario appearing for a smooth continuation by decreasing ω_b along a path B-D-E in figure 1(*a*) is illustrated in figure 2. At the point D, where $\omega_b = \frac{1}{2}\sqrt{1+4C_K}$ ($\approx 0.574\,46$ for $C_K = 0.08$ as in figure 2), the second breather harmonic enters the phonon band, and we observe (figure 2(*a*)) how the previously exponentially decaying breather tail acquires non-decaying oscillations and thus a phonobreather form (cf [13]). The wave vector of the phonon tail corresponds to that of the first resonating phonon, which is the band edge phonon $q = \pi$. By further decreasing the frequency until $\omega_b < 0.5$ and then continuing the solution back to the anticontinuous limit (path D-E-F in figure 1(*a*)), we confirm that the code of the solution for the system of size $N = 20$ is [+ 2 − 2 + 2 − 2 + 2 − 2 + 2 − 2 + 2 − 2 + 1 − 2 + 2 − 2 + 2 − 2 + 2 − 2 + 2 − 2]. We should stress that this continuation from breather to phonobreather is unique and reversible, i.e. starting with a phonobreather with the above code at a point F, the continuation F-E-D-B-A gives back the simple breather at point A. Thus, there is no true bifurcation associated with this breather–phonon resonance in a finite-size system. Instead, the typical behaviour of the Floquet eigenvalues on the unit circle around the point of resonance is as illustrated in figures 2(*b*) and (*c*). Approaching the point D ($\omega_b \approx 0.5745$) from above the eigenvalue pair corresponding to the band edge phonon $q = \pi$ approaches +1 ($\theta = 0$), but instead of colliding they repel each other and move away again from +1 along the unit circle. Thus, at the point where the breather acquires a phonon tail we generally observe an *avoided collision* of Floquet eigenvalues. However, as illustrated in figure 2(*d*), the gap defined by the distance in angle between the pair of eigenvalues at their closest approach decreases when the system size increases, so that the avoided collision approaches a true collision at +1 when the system size goes to infinity. A similar scenario with avoided eigenvalue collisions was also observed [17] for a disordered KG system (with random harmonic oscillation frequencies)

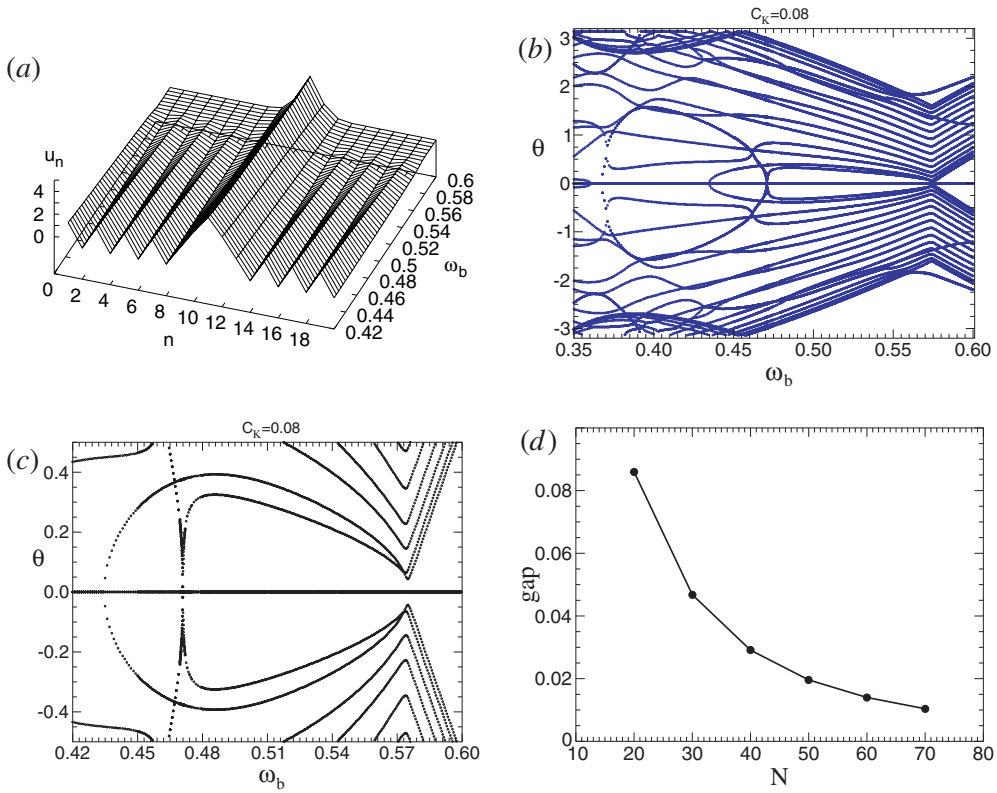

Figure 2. Amplitudes (*a*) and angles of Floquet eigenvalues (*b*), (*c*) for a simple breather penetrating the linear phonon band along a line B-D-E in figure 1(*a*), in a Morse KG system of size $N = 20$ with $C_K = 0.08$. The breather transforms smoothly into a phonobreather at the point $\omega_b \approx 0.5745$ where the avoided eigenvalue collision at $\Lambda = 1$ occurs (enlarged in (*c*)). As shown in (*d*), the size of the 'gap' around $\theta = 0$ at $\omega_b \approx 0.5745$, defined as the smallest difference between the eigenvalue angles $\pm\theta$, decreases with the system size N.

where certain spatially extended multibreathers with frequencies outside the linear band were found to continue smoothly into localized breathers with fundamental frequencies inside the band (which in this case is of pure point nature corresponding to Anderson localized eigenmodes). For the disordered model, the avoided eigenvalue collisions were found not only when the fundamental frequency entered the band but also at each discrete resonance frequency inside the band, and in fact this cascade of avoided collisions was shown to be the signature of a 'good' choice of coding sequence for the initial multibreather, in order to be continuable to a strictly localized intraband breather [17].

There are some other points worth mentioning concerning the smooth breather–phonobreather transition observed here. One interesting observation is that if the path of the eigenvalues corresponding to the avoided collision in figure 2 is followed for the phonobreather towards smaller frequencies, they will eventually approach +1 again, and finally a true eigenvalue collision at +1 is realized (at $\omega_b \approx 0.4346$ in figures 2(*b*) and (*c*) for $C_K = 0.08$), after which the eigenvalues go out on the real axis and create an instability for the phonobreather. The location of this collision is essentially independent of the system size. In appendix A we use the technique of *band analysis* [1] to better understand the origin of this behaviour. There is also another eigenvalue collision at +1 (at $\omega_b \approx 0.4711$ in

figures 2(*b*) and (*c*)) where a pair of eigenvalues goes out on the real axis and yields an additional instability. This corresponds to a resonance with the next phonon mode, which is antisymmetric around the central breather site [19]. However, we should stress that it is possible to perform the full breather–phonobreather continuation A-B-D-E-F in figure 1(*a*) without encountering *any* collisions at +1, by keeping C_K small on the path B-D-E and ω_b close to 0.5 on the path E-F.

Let us also remark that, as we use periodic boundary conditions, the scenario will be slightly different for odd number of sites N than as shown in figure 2 for N even. Namely, for odd N the first eigenmode corresponding to the band edge linear phonon $q = \pi$ will be antisymmetric with respect to the central breather site (where the mode necessarily has a defect in the sequence of alternating signs) and thus it does not couple to the symmetric breather. As a consequence, we will observe a true eigenvalue collision at +1 close to the point D, which produces a narrow regime of instability (the analogue of the antisymmetric resonance for $N = 20$ described above), but no breather–phonobreather transition. This transition instead occurs at the next phonon resonance, with a resonating phonon mode whose coding sequence has a defect at the boundary compared to the pure π-phonon, making it symmetric around the breather centre. Also in this case, the breather–phonobreather transition is signalled by an avoided eigenvalue collision [19].

An example of the continuation along a path A-B-C (i.e., by increasing the coupling at constant frequency) is shown in figure 3. The initial scenario for the smooth continuation of the simple breather into a phonobreather with a $q = \pi$ phonon tail is just as described above. Then, as seen in figure 3(*a*), when C_K increases the amplitude of the phonon tail increases while the breather widens and oscillations appear in its shape. At a certain point ($C_K \approx 0.3535$ for $\omega_b = 0.6$ and $N = 60$ as in figure 3), the breather disappears and the phonobreather transforms into a pure $q = \pi$ nonlinear phonon with frequency $2\omega_b$. This transformation is associated with a collision of Floquet eigenvalues at +1 as illustrated in figure 3(*d*) (a period-doubling bifurcation in the direction of decreasing C_K). In fact, exactly at the bifurcation point the numerical Newton method does not converge as the corresponding matrix [17] becomes non-invertible, but this is not observed unless the continuation is performed with extremely small steps in C_K ($\sim 10^{-9}$ or smaller) when approaching this point. The exact location of this bifurcation depends only weakly on the system size, e.g. for $N = 20$ it occurs at $C_K \approx 0.3518$. For a further increase in coupling the phonon amplitude is further amplified, and finally it diverges when $C_K = \omega_b^2$ ($=0.36$ in figure 3). This is a consequence of the shape of the Morse potential (4) which becomes flat for large u, so the amplitude divergence corresponds to the particles leaving their potential wells. In the large-amplitude limit, the phonon dispersion relation can be calculated by neglecting the on-site potential in (3), which yields $\omega_\infty^2(q) = 4C_K \sin^2(q/2)$ in agreement with the numerically observed value for the amplitude divergence when $\omega_\infty = 2\omega_b$ and $q = \pi$.

3.1.2. 'Phantom breathers'. As we have just illustrated above, the smooth continuation of a simple breather in a soft potential generally yields the formation of a phonobreather with a tail corresponding to a $q = \pi$ phonon (possibly with a defect at the boundary) as the second breather harmonic enters the phonon band. However, in principle it is possible to construct phonobreathers with second-harmonic tails having an arbitrary wave vector q, compatible with the system size and the boundary conditions, by continuing solutions from the anticontinuous limit where the tail is generated using (9) for the desired q and $p = 2$. These solutions can however never be reached from a smooth continuation of a simple breather as the linear dispersion curves (8) for general $q \neq \pi, 0$ lie in the interior of the phonon band, and thus any possible resonance leading to the formation of such a phonobreather from a localized breather

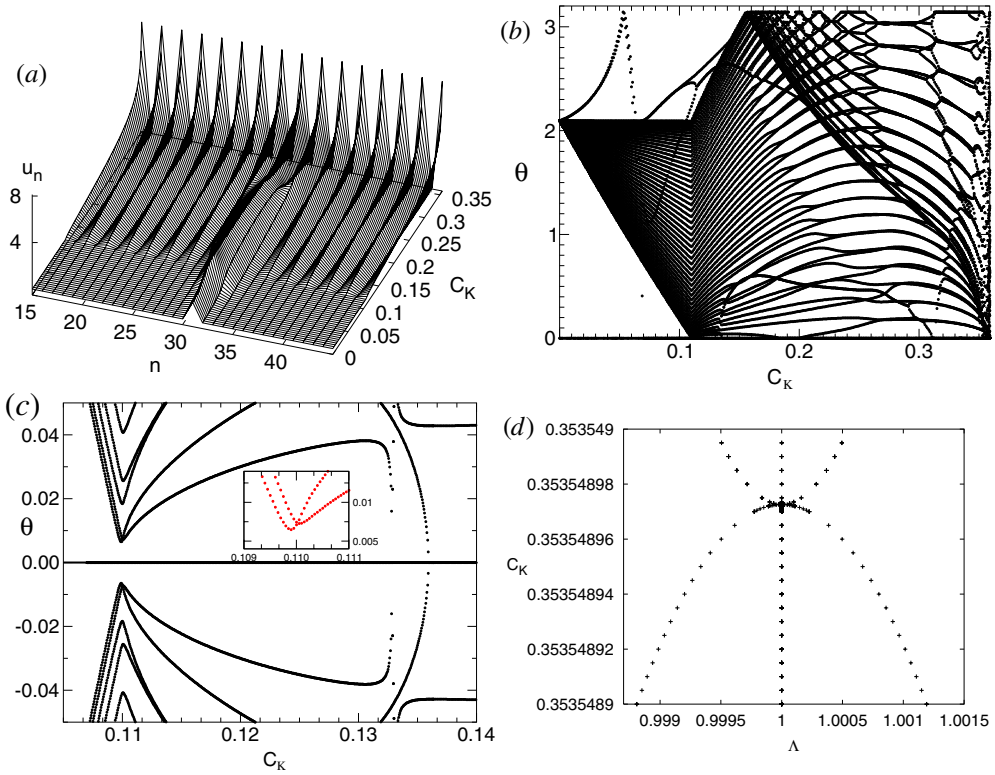

Figure 3. Amplitudes $\{u_n(0)\}$ (a) and angles θ of Floquet eigenvalues (b) for the smooth continuation of a simple breather into the linear phonon band, in a Morse KG system of size $N = 60$, with $\omega_b = 0.6$ and increasing C_K. In (c), enlargement of the regime around the breather–phonobreather transition in (b), the inset shows crossing of bands at the avoided collision; (d) shows the behaviour of eigenvalues on the real axis around the point where the phonobreather transforms into a pure nonlinear phonon with wave vector $q = \pi$.

would necessarily appear *after* the resonance with the $q = \pi$ phonon. Consequently, if we wish to reach a phonobreather with a phonon tail with $q \neq \pi$ by continuation of a simple breather, it is necessary to 'jump' over the regime in parameter space corresponding to resonance with the $q = \pi$ phonon to avoid the breather transforming into a $q = \pi$ phonobreather as described above. Numerically, this can be achieved by tailoring the step-length in C_K or ω_b so as to be large enough to jump over the resonance regimes, but small enough to yield convergence to a solution close to the initial one. Now, as discussed in the introduction and also briefly in [13], the fact that for a not too large finite system the linear dispersion curves will be rather sparsely distributed opens the possibility for an interesting scenario: if one dispersion curve is successfully 'jumped over', there may still be an interval left before the next dispersion curve is reached, and in this interval we could expect to find a solution which is practically localized. Such a solution will be called a 'phantom breather'.

An example of solutions generated through this technique in its simplest fashion, by following a path B-D-E in figure 1(a) with steps of constant length -0.01, is given in figure 4(a). We note that inside the phonon band ($0.5 < \omega_b < 0.5745$) we generally find solutions with small-amplitude tails, but the amplitude of the tails, as well as their wave vectors, clearly varies as the phonon band is traversed. Now, each solution found through this technique can be identified by *smoothly* continuing it through the phonon band and then along

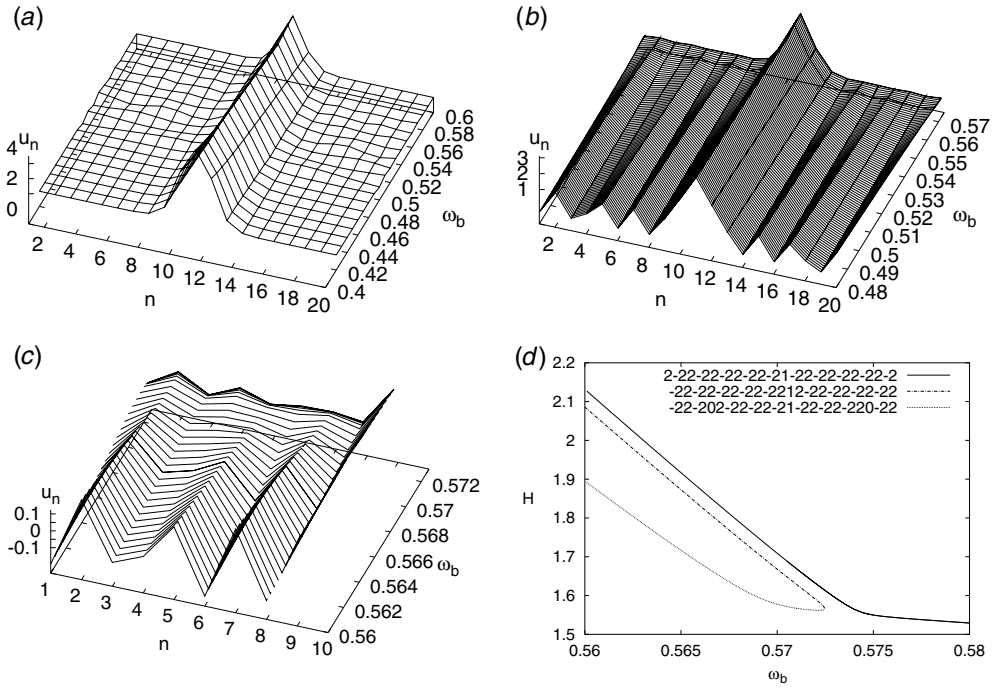

Figure 4. (*a*) Sequence of exact 'phantom breather' solutions found numerically in a Morse KG model with $N = 20$ by starting from a simple breather at $\omega_b = 0.6$ and traversing the second-harmonic phonon band at constant coupling ($C_K = 0.08$) with large frequency steps (-0.01). (*b*) Smooth continuation of the first phantom breather inside the band in (*a*), both towards smaller ω_b into the phonobreather $[-22-202-22-22-21-22-22-220-22]$ and towards larger ω_b until it bifurcates with the phonobreather with code $[-22-22-22-22-2212-22-22-22-22]$ at $\omega_b \approx 0.572\,47$. (*c*) Enlargement of the tail in (*b*) (note the new oscillations that appear when increasing ω_b approaching the bifurcation point). (*d*) Total energy (2) versus ω_b for the two phonobreathers connecting to the phantom breather, as well as for the phonobreather connecting to the pure breather (solid line) as described in figure 2. The 'phantom breather' regime of small-amplitude tails corresponds to the flatter part of the lower curve ($0.571 \lesssim \omega_b \lesssim 0.572$).

a path E-F down to the anticontinuous limit where its multibreather coding sequence can be found. Of course, the sequence of multibreathers found in this way is rather arbitrary, since the initial step length was chosen at random, but still some interesting remarks can be made already from this simple experiment. We note for example that after the traversal of the phonon band we have again a localized solution, but, in contrast to what might have been expected, this solution is not a simple breather but a multibreather having a block $[+2-2+1-2+2]$ of five central sites with non-zero codes. In fact, this central block, with possible reversal of the signs for the second-harmonic sites, is found for all the solutions in figure 4(*a*). Another general remark is that the tails typically consist of alternating codes +2 and -2 (occasionally with two identical codes at the boundary), but with one or several symmetrically placed pairs of 'defect' sites of code 0 interjected. The number of zeroes in the codes generally increases as the phonon band is traversed towards lower ω_b. Thus, these tails have similar properties to the nonlinear standing-wave phonons generated by (9), although they in general for a finite-size system do not have a clearly defined wave vector q.

Let us now look more carefully at this scenario. In figure 4(*b*) we show the smooth continuation of the first intraband solution found in figure 4(*a*), i.e. the solution appearing after

the resonance with the $q = \pi$ phonon at the band edge $\omega_b \approx 0.5745$ has been jumped over. Decreasing ω_b the tail amplitude increases, and following the solution down to $C_K = 0$ for $\omega_b < 0.5$ yields the phonobreather coding sequence given in the figure caption, which contains one symmetric pair of 'defect' zeroes. On the other hand, attempts to continue it towards larger ω_b fail at a certain point ($\omega_b \approx 0.572\,47$), where it bifurcates with the phonobreather solution having a $q = \pi$ tail, but with all codes ± 2 having *opposite* signs compared to the phonobreather formed by smooth continuation of the pure breather (cf figure 2). The bifurcation scheme in the energy versus frequency plane is shown in figure 4(*d*). Looking more carefully at the amplitude of the tail of the solution (figure 4(*c*)), we can identify a transition regime where the shape of the tail oscillations changes from those characteristic of one of the two bifurcating solutions to those characteristic of the other. In this transition regime ($0.571 \lesssim \omega_b \lesssim 0.572$ in this example) the tail amplitude is very small and thus the solution here has the characteristics of a phantom breather. In the energy diagram (figure 4(*d*)) this regime is identified by the flat part of the lower (dashed) curve, which approximately is in continuation of the energy curve corresponding to the pure breather (solid curve for $\omega_b > 0.5745$).

The properties observed above can be generalized to obtain a systematic way of generating a whole class of solutions of phantom breather type. We will illustrate this procedure further by the example shown in figure 5 for a path A-B-C at constant frequency. Figure 5(*a*) shows the smooth continuation of the solution obtained by jumping over the *two* first phonon resonances, i.e. those yielding the $q = \pi$ phonobreather and the phonobreather in figure 4(*b*). As before, we obtain the coding sequence of this solution by continuing it towards smaller frequency until $\omega_b < 0.5$ and then towards smaller coupling until $C_K = 0$, and thus find a code with *two* symmetric pairs of defect zeroes in the sequence of alternating ± 2 codes (see caption of figure 5). As is clearly visible in figure 5(*a*), for these parameter values this solution has a significant phantom breather regime ($0.122 \lesssim C_K \lesssim 0.142$) where the tail amplitude is negligible compared to the breather amplitude (see also tail enlargement in (*c*)). Moreover, we note that the scenario by which the tail oscillations start to grow when increasing C_K is similar to the scenario for the pure breather–phonobreather transition (figure 3), and also here associated with an avoided collision of Floquet eigenvalues at +1 (figure 5(*b*)). In fact, as the coding sequence for the tail of the solution contains repeated units $[+2\ -\ 20]$ it is close to that of a standing-wave phonon with wave vector $q = 2\pi/3$ (cf (9)), and the numerically observed value for the avoided collision ($C_K \approx 0.142$) is also close to the value $C_K = \frac{(2\omega_b)^2-1}{4\sin^2(q/2)} \approx 0.1467$ obtained from (8) for a linear phonon resonance at $q = 2\pi/3$.

On the other hand, continuing the solution in figure 5 towards smaller coupling, we find, analogously to the scenario in figure 4, that the oscillatory characteristics of the tail change (figure 5(*c*)), and at a certain point (here $C_K \approx 0.122\,18$) the continuation stops as the solution bifurcates with another phonobreather whose code is given in the caption of figure 5. Now, comparing the code of this solution with the code of the solution obtained immediately after jumping over the first resonance (figure 4), we find that they are identical except for having all signs ± 2 reversed. Thus, the scenario is equivalent to that observed for the bifurcation of the solutions connecting to the first phantom breather in figure 4. We summarize the bifurcation scheme for the first three breather–phonon resonances by plotting the corresponding energy-coupling diagram in figure 5(*d*). In this figure, each phantom breather corresponds to the flat part of the energy curve connecting two particular phonobreathers, and for each phantom breather the code of the phonobreather connecting from smaller coupling is obtained by reversing the signs of all codes ± 2 in the code of the phonobreather connecting to the *previous* phantom (or pure) breather from higher coupling. This procedure repeats itself, and thus we have a class of phantom breathers which all have small-amplitude tails in the transition regime between the two connecting phonobreathers.

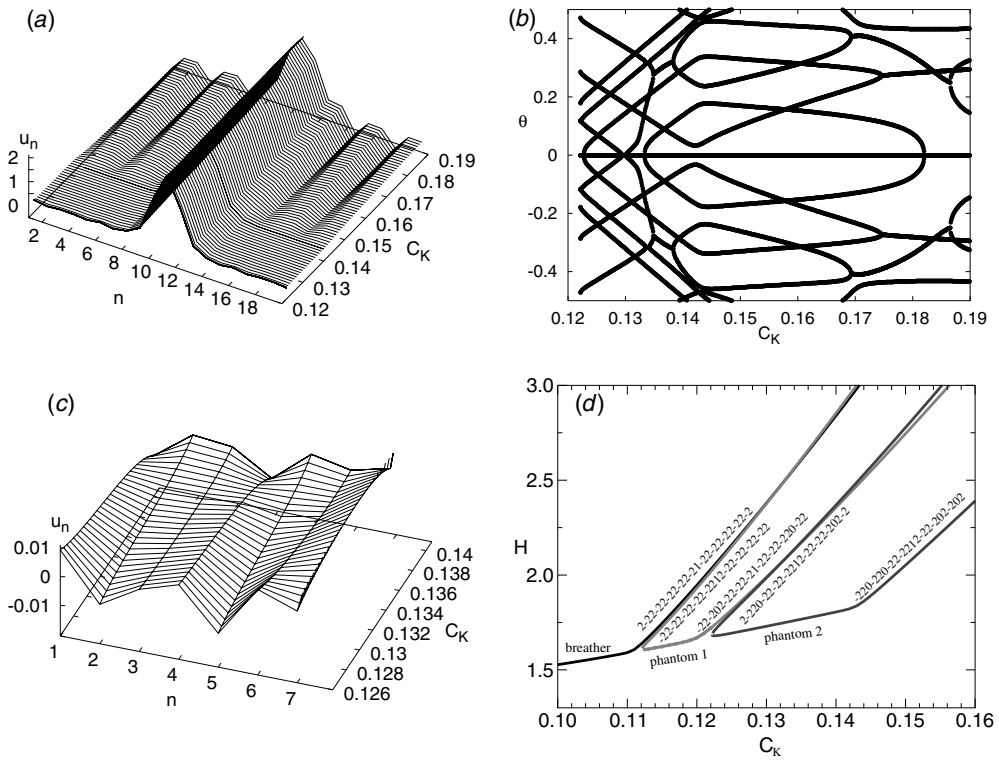

Figure 5. (*a*) Smooth continuation at constant frequency $\omega_b = 0.6$ of the second intraband phantom breather in a Morse KG system with $N = 20$, forming the phonobreather with code [−220 − 220 − 22 − 2212 − 22 − 202 − 202] for increasing coupling and bifurcating with the phonobreather with code [2 − 220 − 22 − 22 − 2212 − 22 − 22 − 202 − 2] for decreasing coupling (at $C_K \approx 0.122\,18$). (*b*) Variation of the angles of the Floquet eigenvalues for the continuation in (*a*) (note the avoided collision at $\theta = 0$ at the same point ($C_K \approx 0.142$) where the phonon tail in the amplitudes in (*a*) becomes visible). (*c*) Enlargement of the tail in (*a*) in the phantom breather regime (note the gradual change of nature of the tail, which becomes almost flat for $C_K \approx 0.137$). (*d*) Total energy (2) versus C_K for the continuation of (i) (black line) a simple breather into a $q = \pi$ phonobreather (cf figure 3); (ii) (light gray line) the two phonobreather solutions connecting to the first phantom breather ('phantom 1') (cf figure 4); (iii) (dark gray line) the two phonobreather solutions connecting to the second phantom breather ('phantom 2') as in (*a*)–(*c*) above.

Let us also briefly comment on the stability of the phantom breather solutions. In fact, for the particular choices of parameter values used in figures 4 and 5 they are generally unstable, but these instability mechanisms are not a particular characteristic of the phantom breathers but occur also for the pure breathers before the second harmonic enters the phonon band for these values of C_K respectively ω_b [22, 23]. Performing, for example, the corresponding continuation as in figure 4(*b*) but for the smaller value of the coupling $C_K = 0.05$, we typically find linearly stable phantom breathers. However, in some cases additional instability mechanisms may also occur for the phantom breathers. These may be associated with resonances with phonon-modes antisymmetric with respect to the breather centre, which do not yield phonobreathers appearing in the cascade of bifurcations illustrated in figure 5(*d*), but typically cause narrow regimes of instabilities through eigenvalue collisions at +1 (see an example in figure 5(*b*) for $C_K \approx 0.1295$–0.1300). Also additional oscillatory instabilities (i.e. complex eigenvalues appearing from eigenvalue collisions on the unit circle) such as those found for the pure

standing-wave phonons [20, 21] may appear for the phantom breathers, but as long as the tail amplitude is small they are weak and only appear in narrow parameter regimes. On the other hand, in the pure phonobreather regime with large tail amplitudes, these instabilities may be considerable as can be seen in figures 3(*b*) and 5(*b*) (they are identified in these figures as two curves merging at the point where the eigenvalue pair leaves the unit circle, and splitting when the pair returns).

3.1.3. Vanishing of the tail. The scenario described in the previous section and summarized in figure 5(*d*) generally occurs when varying one parameter (e.g. frequency or coupling) while keeping all others fixed. The tail of the phantom breathers found in the transition regime between two neighbouring phonobreathers changes in the transition, for, though its amplitude might be very small as in figure 5(*c*), it is typically non-zero even at the point where it attains its minimum. However, by considering variations of both frequency and coupling, we might find special parameter values where the tail completely vanishes and the phantom breather becomes exponentially localized for the whole system. To analyse the origin of this behaviour, we reconsider the scenario in figure 5 by performing the continuation towards smaller frequencies for the 'phantom 2' solution for different values of the coupling in its existence regime. One could then expect to find generally the same scenario as for the continuation towards larger coupling in figure 5; however, this does not turn out to be the case. By contrast, we find that the expected continuation of the phantom breather into the phonobreather with the oscillation pattern given in figure 5 only occurs if $C_{\mathrm{K}} > C_{\mathrm{K}}^{(\mathrm{cr})} \approx 0.135\,774\,8$; for smaller values of the coupling the phonon oscillations of the resulting phonobreather will have *opposite phases* (i.e. codes $\pm 2 \to \mp 2$). Thus, exactly at the point $C_{\mathrm{K}} = C_{\mathrm{K}}^{(\mathrm{cr})}$ where the phantom breather 'changes phonobreather', the oscillations from the two antiphased phonons should cancel each other and leave a completely localized phantom breather. Investigating this scenario in detail below shows that this indeed is the case.

We show in figure 6 the bifurcation scenario in the energy versus frequency plane for some values of the coupling around the critical value $C_{\mathrm{K}}^{(\mathrm{cr})}$. As mentioned above, for $C_{\mathrm{K}} < C_{\mathrm{K}}^{(\mathrm{cr})}$ the continuation of the second phantom breather towards lower frequencies yields a phonobreather with code [2 − 202 − 202 − 22 − 21 − 22 − 220 − 220 − 2], i.e. having $\sigma_1 = +2$ (opposite to that in figure 5). When C_{K} is considerably smaller than $C_{\mathrm{K}}^{(\mathrm{cr})}$, the energy diagram (figure 6(*a*)) has the structure of an avoided pitchfork bifurcation analogous to figure 4(*d*), and, for ω_{b} close to the resonance, the energy of the above phonobreather connecting to the second phantom breather is larger than that of the next (third) phantom breather and the two phonobreathers connecting to it. However, for smaller ω_{b} the energy curves corresponding to two phonobreathers with the phonon parts in antiphase (here, the solution above with $\sigma_1 = +2$ and the solution [−220 − 220 − 22 − 2212 − 22 − 202 − 202] with $\sigma_1 = -2$) might cross, as is seen in figure 6(*a*) (and also for two other cases in figure 5(*d*) for increasing coupling). In general, even though the energies of the two solutions coincide at the crossing the amplitude patterns do not, and thus the point of crossing is generally not a point of bifurcation. Now, increasing C_{K} approaching $C_{\mathrm{K}}^{(\mathrm{cr})}$ the energy curves for phantom 3 and the phonobreather with $\sigma_1 = -2$ will move in the direction of larger ω_{b} (to the right in the figures relative also to the curve for phantom 2 and its phonobreather), and consequently the crossing of the energy curves will occur for smaller and smaller energies (i.e. move downwards in the figure). At a certain value of C_{K} the situation illustrated in figure 6(*b*) is reached, where the point of crossing has passed the point of bifurcation between phantom 3 and the $\sigma_1 = -2$ phonobreather, so that for somewhat larger coupling both solutions will have the characters of phantom breathers (i.e. with very small tail)

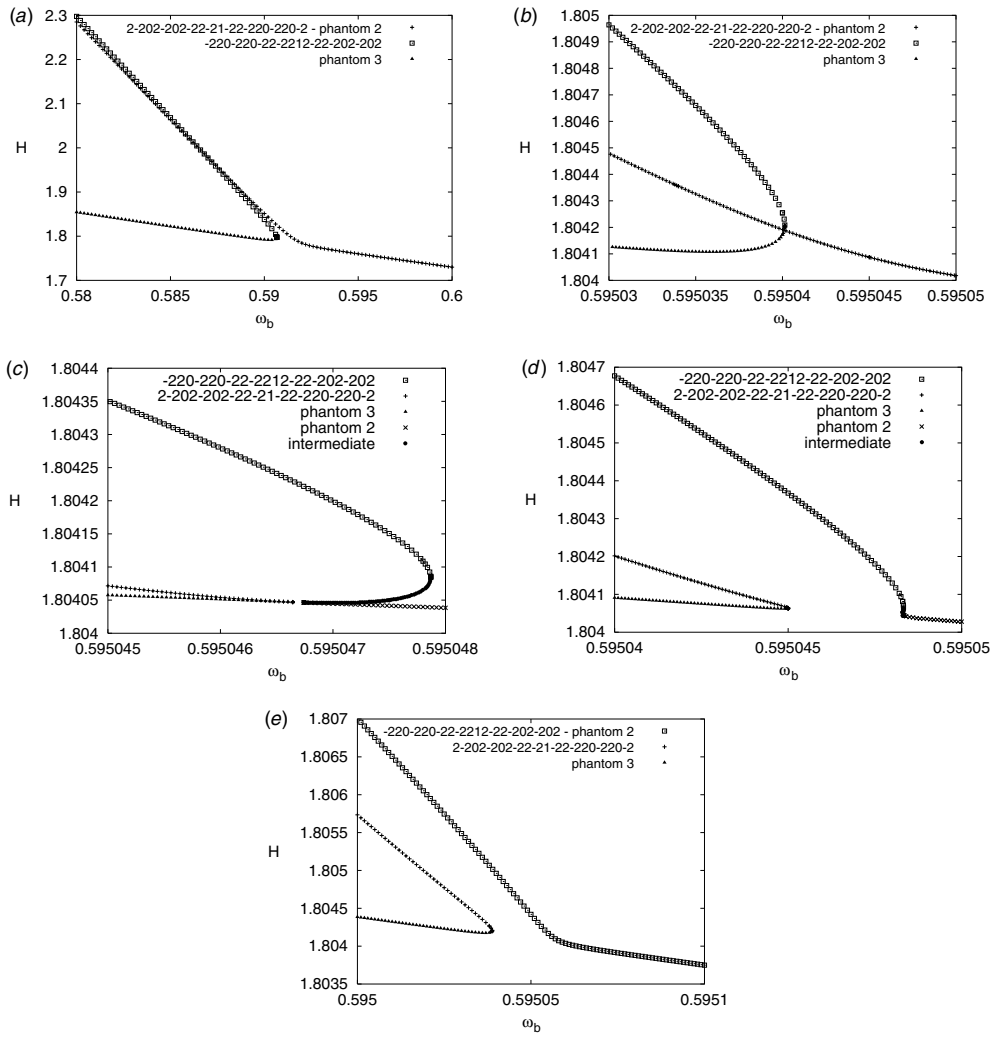

Figure 6. Bifurcation scheme showing total energy (2) versus frequency ω_b for five different values of the coupling C_K around the critical value $C_K^{(cr)} \approx 0.135\,7748$, where the phonon part of the phonobreather in continuation of the 'phantom 2' solution in figure 5 changes sign. In (*a*) $C_K = 0.13$, in (*b*) $C_K = 0.135\,77$, in (*c*) $C_K = 0.135\,7748 \gtrsim C_K^{(cr)}$, in (*d*) $C_K = 0.135\,775$ and in (*e*) $C_K = 0.135\,78$. In the leftmost part of the figures the solutions are, from above, the phonobreathers with codes $[-220-220-22-2212-22-202-202]$ and $[2-202-202-22-21-22-220-220-2]$, respectively, and the third phantom breather continuing towards smaller ω_b until the next resonance. In the rightmost part of the figures the only solution is the second phantom breather, while in (*c*) and (*d*) also an intermediate solution appears connecting the second phantom breather with the phonobreather $[-220-220-22-2212-22-202-202]$. Note that there are no bifurcations at the points of crossing of curves in (*a*) and (*b*); even though the solutions at this point have the same energy they are not identical. Note also the tiny gap around $\omega_b \approx 0.595\,0466$ in (*c*) which closes exactly at $C_K = C_K^{(cr)}$.

rather than phonobreathers when their energy coincide. Increasing further the coupling yields a critical value, $C_K = C_K^{(cr)}$, where also the slopes of the two energy curves become equal at the point where they cross. At this point, there is a true bifurcation and the solutions are

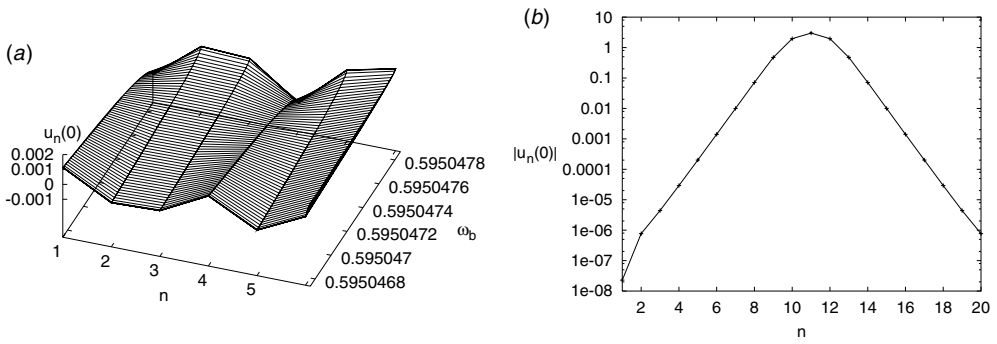

Figure 7. (*a*) Tail of the solutions belonging to the intermediate branch of the Z-shaped part of the energy curve in figure 6(*c*) (in full scale the solutions are practically indistinguishable from the phantom breather part of figure 5(*a*)). (*b*) Logarithmic plot of the solution in (*a*) with the smallest tail, appearing for $\omega_b \approx 0.595\,047\,4592$ (note the almost perfect exponential decay).

identical. For C_K close to, but larger than, $C_K^{(cr)}$ the situation illustrated in figure 6(*c*) appears. Now, the two phantom breathers have interchanged their connecting phonobreathers, so that phantom 3 connects to the phonobreather with $\sigma_1 = +2$, while phantom 2 connects to the phonobreather with $\sigma_1 = -2$. However, here the latter connection does not appear through monotonic continuation versus frequency but only indirectly via an intermediate branch, thus creating a zig-zag-like, *Z-type*, energy diagram. Increasing further C_K the Z-part straightens and the intermediate regime shrinks (figure 6(*d*)), and finally (figure 6(*e*)) there is again a monotonic continuation of phantom 2 into a phonobreather as for $C_K < C_K^{(cr)}$, but now into the phonobreather with $\sigma_1 = -2$ (as in figure 5).

It is interesting to note that a similar bifurcation pattern was observed recently in a different context in a study of discrete breathers in anisotropic ferromagnetic spin chains [24]. Investigating for this model the continuation of discrete multibreathers into the continuum magnetic soliton, it was found that when varying some parameter the continuum soliton could continue into different possible multibreathers, and the bifurcation scenario switching the multibreather connecting to the soliton was similar (although not completely identical) to the scenario switching the phonobreather connecting to the phantom breather in our model (compare figure 6 here with figure 6 of [24]).

Let us now consider the shape of the tail of the solution belonging to the intermediate part of the Z-type curve in figure 6(*c*), i.e. very close to the critical value $C_K^{(cr)}$. In figure 7(*a*) we show how the tail varies along this branch. It is apparent that going from the smallest to the largest values of ω_b in its existence regime, the oscillation pattern of the six first sites changes from [2 − 202 − 20] to [−220 − 220] (the amplitudes of the rightmost sites are relatively larger due to the exponential decay of the central breather part). Thus, in passing from these two antiphased phonon tails, the solution should pass through a point of zero amplitude tail at some intermediate frequency, where the contributions from the two antiphased phonons cancel leaving only the exponentially decaying part coming from the central breather. That this indeed happens is illustrated in figure 7(*b*), showing a practically perfect exponential decay over the whole system, with the exception of the three central sites and the boundary site $n = 1$. In fact, strictly speaking there is an undisturbed smooth continuation between the two phonobreathers [2 − 202 − 202 − 22 − 21 − 22 − 220 − 220 − 2] and [−220 − 220 − 22 − 2212 − 22 − 202 − 202] only at $C_K = C_K^{(cr)}$, since this is the only case where the two solutions connect without interruption. Thus,

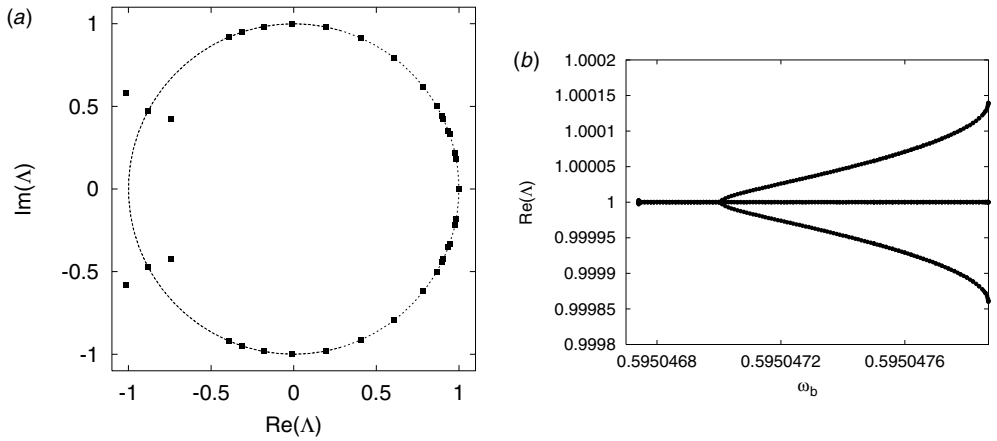

Figure 8. (*a*) Floquet eigenvalues for the solutions belonging to the intermediate branch of the Z-shaped part of the energy curve in figure 6(*c*) (on this scale the eigenvalues for all solutions on this branch appear identical). (*b*) Magnification of the region around $\Lambda = 1$ in (*a*), with the real part of Λ plotted as a function of frequency.

only exactly at $C_K = C_K^{(cr)}$ should we expect the tail to completely vanish; going away from this exact value the tail will also have some contribution from the other phonobreathers connecting to the phantom breather (as in figures 4(*c*) and 5(*c*)). However, as shown in figure 7, also for C_K very close to, but not exactly at, the critical value, the family of solutions belonging to the intermediate branch of the Z-shaped energy curve corresponds almost exactly to a pure transition between the two antiphased solutions (with only a very weak influence from the solution connecting to phantom 2 from higher frequencies), and thus this family contains an almost perfectly exponentially localized solution at some ω_b as shown in figure 7(*b*).

Let us also comment on the stability of the solutions belonging to the intermediate branch of the Z-shaped curve for $C_K \gtrsim C_K^{(cr)}$. The eigenvalues of the Floquet matrix for these solutions for $C_K = 0.135\,7748$ are shown in figure 8. As is seen in figure 8(*a*) there is all the time a quartet of rather large complex eigenvalues outside the unit circle, and thus the solutions are always unstable through oscillatory instabilities. However, these instabilities are not characteristic only of this branch of solutions, rather they appear for all related solutions with similar values of C_K and ω_b (e.g. all solutions represented in figure 6). Thus, as they are practically independent of the nature of the tails, the oscillatory instabilities originate in resonating internal oscillations around the central breather sites. However, looking more closely around the point $\Lambda = 1$ we find also (figure 8(*b*)) additional very weak real instabilities but only for a part of the intermediate regime. These stability changes are related to a change of the slope of the corresponding energy curve (figure 6(*c*)), and the additional real instabilities appear when $dH/d\omega_b > 0$. In particular, we see that the solution with the minimal tail in figure 7(*b*) is weakly unstable also through these real instabilities.

We end this part with a more general remark. Although in general (except at critical points $C_K^{(cr)}$) it is not possible in a smooth way to continue one phantom breather through a resonance regime into another phantom breather by monotonic variation of one parameter, the existence of critical points $(\omega_b^{(cr)}, C_K^{(cr)})$ in the (ω_b, C_K) plane renders possible a smooth continuation of one phantom breather to the next by continuing along a path which encircles the critical point. For example, starting with the second phantom breather and continuing it

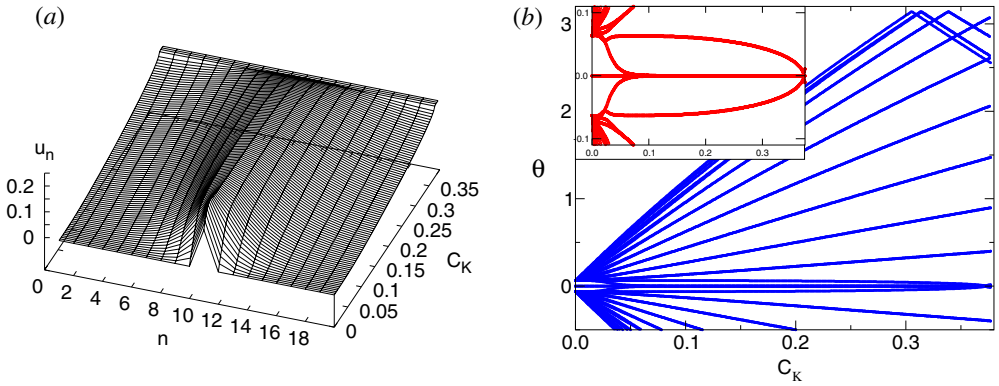

Figure 9. Amplitudes (*a*) and angles of Floquet eigenvalues (*b*) (the inset in (*b*) shows enlargement of the zone close to $\theta = 0$) for continuation versus coupling at fixed $\omega_b = 0.99$ of a simple breather in a Morse potential KG chain of $N = 20$ oscillators.

towards larger coupling into the phonobreather with $\sigma_1 = -2$ as in figure 5, we can then, for fixed $C_K > C_K^{(cr)}$, continue it towards smaller ω_b and then again towards smaller C_K for some fixed $\omega_b < \omega_b^{(cr)}$ until it connects with the third phantom breather at some $C_K < C_K^{(cr)}$ as in figures 6(*a*) and (*b*).

3.1.4. First harmonic $q = 0$ resonance. In the previous sections, we have chosen the breather frequency ω_b sufficiently small so as to have the oscillation amplitude, as governed by the exponential decay of the fundamental harmonic, negligibly small at the boundaries at the point where $2\omega_b$ enters the linear phonon band. However, if we consider frequencies close to the lower band edge $\omega_b = 1$ for small systems, the scenario of breather–phonon resonances might be different from that described above, since the breather already for small couplings will spread out over a large part of the system and have a considerable amplitude at the boundaries. In particular, the breather might then bifurcate with the nonlinear band edge $q = 0$ phonon before the regime of second-harmonic resonances is reached. This scenario is illustrated in figure 9, where we have chosen a frequency very close to the linear phonon band edge, $\omega_b = 0.99$, and a rather small system, $N = 20$. As the coupling is increased the breather gradually spreads over all the system and loses its characteristic tail exponentially decaying towards zero. At a certain point ($C_K \approx 0.372\,122$ in figure 9) the breather bifurcates with the $q = 0$ nonlinear phonon, and for larger couplings a constant-amplitude state is reached (with an amplitude identical to that of uncoupled oscillators with frequency ω_b). This bifurcation is signalled by a collision at +1 in the Floquet eigenvalue spectrum (figure 9(*b*)) and, in fact, exactly at the bifurcation point the numerical scheme does not converge due to non-invertibility. However, similar to the transformation of a phonobreather into a pure nonlinear phonon in figure 3, the non-convergence is typically not observed unless a very small step-length is used.

Thus, for the small system in figure 9 the breather transforms into a constant-amplitude state before reaching the linear second-harmonic resonances, which for $\omega_b = 0.99$ appear only for $C_K > 0.7301$. However, the value of C_K where the $q = 0$ resonance occurs increases quite rapidly with the size of the system, so that when $N \gtrsim 30$ the breather still has a localized (although wide spread) character when the regime of second-harmonic resonances is entered for $\omega_b = 0.99$.

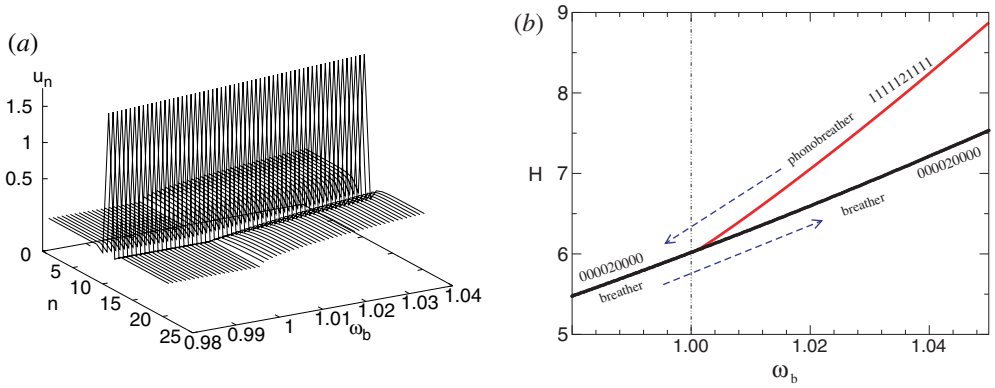

Figure 10. (*a*) Amplitudes $u_n(0)$ for the continuation towards smaller frequency ω_b of the $q = 0$ phonobreather [...1112111...] in a quartic KG system with $N = 21$ and $C_K = 0.1$. At $\omega_b = 1$ the tail amplitude goes to zero and the phonobreather transforms into the simple breather [...0002000...]. (*b*) The breather–phonobreather bifurcation in the plane (ω_b, H). The lower (black) curve shows the energy of the breather, the upper (grey) curve the energy of the phonobreather.

3.2. The quartic potential

We will here briefly discuss the generation of phonobreathers in the case of hard potentials, and choose the quartic potential (5) as an explicit example. The scenario is different from that of a soft potential since also the fundamental harmonic now necessarily lies above the linear band, and thus in the continuation the fundamental harmonic will always reach the phonon band before the higher harmonics do. Thus, we will not observe the smooth transition of a breather into a phonobreather, phantom breathers, etc discussed in section 3.1; instead, the breather amplitude will just decay to zero as the fundamental frequency reaches the band. However, as mentioned in section 2, we can still construct phonobreathers from the anticontinuous limit at $\omega_b > 1$, e.g. by choosing a central breather site with code $|\sigma_n| = p'$ and a standing-wave phonon tail with wave vector q generated using (9) (and the transformation below this equation) with $p < p'$. In the simplest case, we can choose $p' = 2$ and $p = 1$. Then, continuing such a solution first towards higher coupling at constant frequency and then towards lower frequency at constant coupling, we expect the tail amplitude to vanish at the point where the linear dispersion curve (8) for frequency $p\omega_b$ and wave vector q is reached. This scenario is illustrated in figure 10 for a single-site breather with $p' = 2$ embedded in a $q = 0$ phonon tail with $p = 1$, which disappears for $\omega_b < 1$ as the phonobreather transforms into a simple breather with frequency $2\omega_b$. Thus, viewed in the direction of increasing frequency, there is a period-doubling bifurcation at $\omega_b = 1$, constituting a complete pitchfork as shown in figure 10(*b*) (the two phonobreather solutions with central codes ± 2 have identical energy due to the symmetry of the potential). This is also seen in the Floquet spectrum as a collision at $+1$ for the continuation with period $T_b = 2\pi/\omega_b$ or at -1 in the continuation of the simple breather at its fundamental period $T_b/2$.

4. Conclusions

In conclusion, we have investigated by numerical continuation techniques several types of exact solutions resulting from interaction between nonlinear localized (breather) and extended

(phonon) modes in finite-size closed chains of Klein–Gordon type. For the case of a soft (Morse) on-site potential, we have analysed the transition from a localized breather into a non-localized phonobreather with a small-amplitude tail as a higher breather harmonic enters the linear phonon band [13]. The breather–phonobreather transition occurs progressively in finite-size systems, and becomes a sharp bifurcation only in the limit of infinite system size. We have also calculated numerically exact practically localized breather-like solutions with frequency harmonics residing inside the linear phonon band, in-between the linear dispersion curves which may be sparsely distributed if the system size is relatively small. These solutions, which we term 'phantom breathers', correspond to the 'intraband breathers' found earlier for disordered systems [18], but in contrast to the latter the phantom breathers in a homogeneous system generically are not exponentially localized but have a small-amplitude tail with a pattern corresponding to a neighbouring phonon mode. The phantom breathers occur in the transition regime between two neighbouring, bifurcating phonobreathers with tails of different coding sequences, and, as for the transition between the pure breather and the band edge phonobreather, the transition between a phantom breather and its neighbouring phonobreathers is not distinct but occurs gradually. However, for special parameter values we find that the phantom breather connects simultaneously to two phonobreathers with phonon parts having the same pattern but oscillating with opposite phases; in this case the phonon tails may exactly cancel and leave a phantom breather which is exponentially localized for the whole system. This mechanism is reminiscent of that leading to 'embedded solitons' in continuous systems (see, e.g., [25]). Considering briefly the case of a hard (quartic) on-site potential, where the scenario necessarily is different since all harmonics (including the fundamental) lie above the phonon band, we constructed phonobreathers from the anticontinuous limit and showed how they appear from period-doubling bifurcations in the continuation of a simple breather when half the breather frequency enters the linear phonon band.

We remark that generally, the small-amplitude tails of the exact phantom breather solutions appearing when one of the higher harmonics of the fundamental breather frequency is inside the phonon band, are quasilinear stationary phonons which could be interpreted by the fact that a strictly localized breather solution would radiate energy as a travelling phonon, and thus could not persist as an exact time-periodic solution. Then, to maintain the solution it is necessary to send back another travelling phonon interacting with the breather in order to keep its energy constant. The quasilinear superposition of the outgoing travelling wave and the incoming wave makes the observed tail. Then, from this remark we could calculate the energy radiation of an approximate localized breather by decomposing the tail of the exact phantom breather at its frequency into the superposition of two counterpropagating travelling waves. A formal equation could be obtained in principle from this radiation rate versus frequency for the decay of the breather (cf, e.g., [26]), which ends at the threshold value where there are no harmonics in the phonon band.

Even though we here have concentrated on describing the penetration of a harmonic of a simple breather into the phonon band, similar scenarios should appear for multibreathers, leading analogously to 'phonomultibreathers' and 'phantom multibreathers' in the cases where the original multibreathers are continuable sufficiently far so as to reach the phonon band (in certain cases multibreathers might be lost before through bifurcations). In fact, we have already in [21] (section 5) considered one particular example of this, with the fundamental multibreather itself being a nonlinear standing-wave phonon generated from (9). There we observed the effects of higher-harmonic resonances as a gradual transformation of the wave vector and frequency of the initial wave to those corresponding to the resonating phonon (figures 12 and 16 in [21]). We also found standing waves with the original wave vector existing in-between phonon resonances which, in analogy with the phantom breathers considered here,

could be termed 'phantom standing waves'. We note that, in contrast to the case for simple breathers, these higher-harmonic resonances for standing waves may appear also for hard on-site potentials if the wave vector of the fundamental standing wave is sufficiently small, since then the higher harmonics may reach the phonon band before the amplitude of the fundamental wave goes to zero, which happens only when it reaches its linear dispersion curve inside the phonon band. Some further aspects of higher-harmonic resonances for standing-wave phonons were also considered in [19].

We end with a brief speculation concerning practical applications of our results. Since the phantom breathers appear in finite systems in-between the lines of the phonon spectrum, we do not expect them to be observable in very large systems such as crystals, where the number of atoms is so large that the phonon spectrum is practically continuous. However, there are several examples of real finite systems where discrete breathers are believed to exist, and where also the phantom breather effect could be expected. For example, in molecular systems such as hydrocarbon structures of various sizes, breathers clearly appear in molecular dynamics simulations for realistic parameter values [28, 29], and also resonances with normal modes are observed. Moreover, artificially built devices exhibiting breathers such as arrays of Josephson junctions or coupled waveguides are finite and could involve only a small number of oscillators. A particularly interesting candidate could be quadratic nonlinear photonic crystals of the type described and analysed in [30].

Acknowledgments

A preliminary version of these results was presented at the Nonlinear Lattice Structure and Dynamics Workshop, Dresden, Germany, 24–28 September 2001, and some additional work was stimulated by discussions at this workshop. MJ is supported by the Swedish Research Council and GK by the Greek GSRT.

Appendix A. Band analysis of breather–phonobreather bifurcation

The 'band analysis' technique for analysing and interpreting instabilities and bifurcations found from the Floquet eigenvalue spectrum was introduced and extensively described in [1]; here we give only a very brief summary and an example of its use in the analysis of the breather–phonobreather transition from section 3.1.1. The linearized (Hill) equations (6) can be interpreted as the eigenvalue equations for the 'Newton operator' $\mathcal{N}(\boldsymbol{u}, C_{\mathrm{K}})$,

$$(\mathcal{N}(\boldsymbol{u}, C_{\mathrm{K}}) \cdot \epsilon)_n \equiv \ddot{\epsilon}_n + V''(u_n)\epsilon_n - C_{\mathrm{K}}(\epsilon_{n+1} + \epsilon_{n-1} - 2\epsilon_n) = E\epsilon_n \qquad \text{(A.1)}$$

for the particular eigenvalue $E = 0$. For time-periodic u_n with period T_{b} the eigenvectors of (A.1) fulfil the Bloch condition $\epsilon_n(\theta, T_{\mathrm{b}}) = \mathrm{e}^{\mathrm{i}\theta}\epsilon_n(\theta, 0)$, and the corresponding eigenvalues $E_\nu(\theta)$ are 2π-periodic continuous functions of θ defining, for each ν, a *band* through the dispersion curve $E_\nu(\theta)$. The intersection points of the bands with the axis $E = 0$ yield the Floquet exponents θ_ν (i.e. angles of eigenvalues on the unit circle of the Floquet matrix $\mathbf{F_0}$ defined by (10)), and thus linear stability requires, for a system of N oscillators, to have $2N$ intersections between the bands $E_\nu(\theta)$ and the axis $E = 0$ (counted with their multiplicities). When varying C_{K} or T_{b} the bands evolve, and instabilities appear when bands lose their intersections with $E = 0$.

Figure A1 shows the band spectra close to $(\theta, E) = (0, 0)$ for several parameter values in the regime where the breather–phonobreather transition in figure 2 takes place. In all figures, there is a band tangent to $E = 0$ at $\theta = 0$ corresponding to the 'phase mode' solution

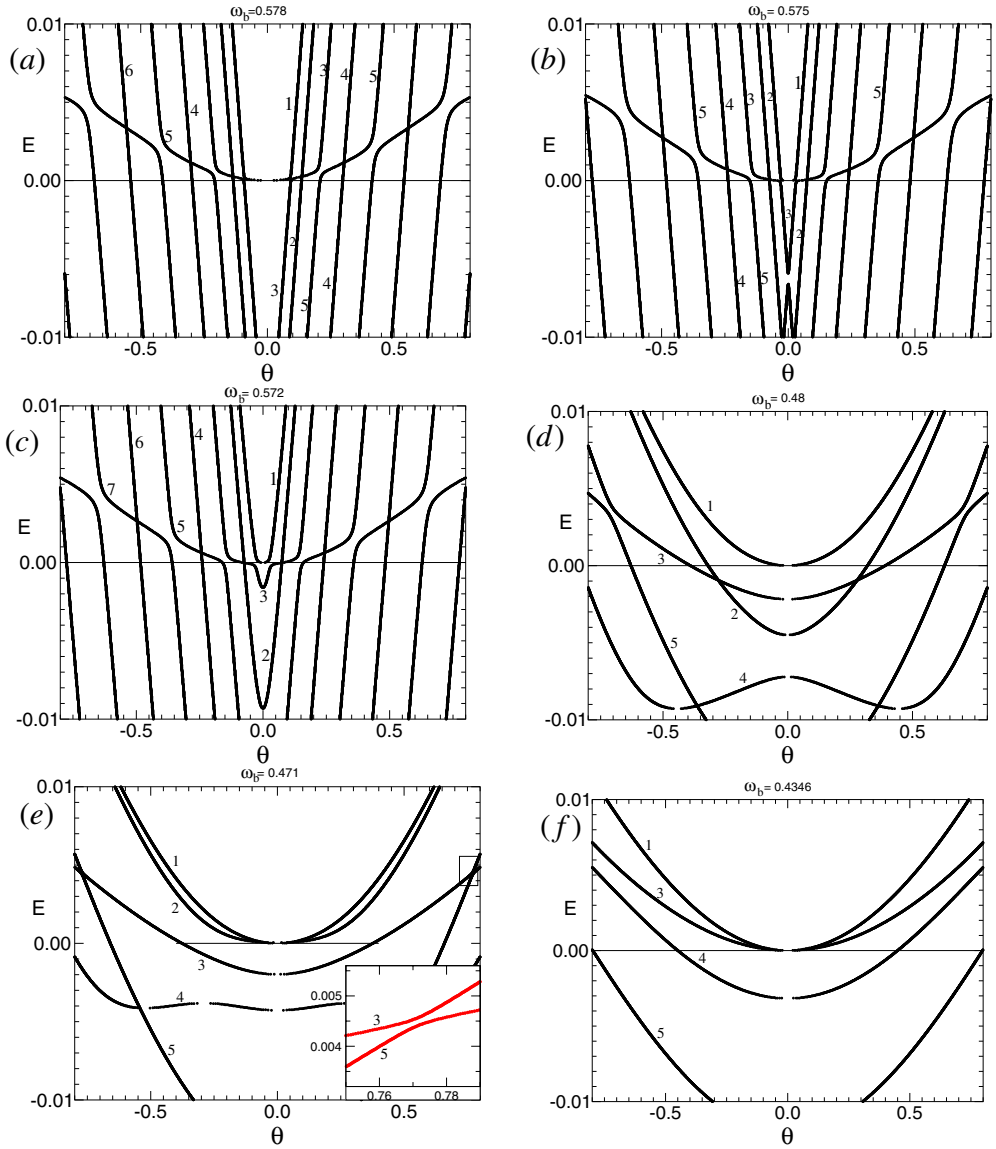

Figure A1. Band spectra for the formation of a phonobreather from a breather in figure 2. (*a*), (*b*) and (*c*) show the spectra around the avoided collision of Floquet eigenvalues at +1 occurring for $\omega_b \approx 0.5745$ (note the gradual change of forms of the bands close to $\theta = 0$); (*d*) $\omega_b = 0.48$ shows the gradual rise of band '2' which, (*e*) at $\omega_b = 0.4711$, cuts the axis $E = 0$ (collision at +1 in figure 2(*c*)) and yields an instability; (*f*) band '3' finally cuts $E = 0$ corresponding to the true collision at +1 observed in figure 2(*c*) at $\omega_b \approx 0.4346$. The apparent gaps within the bands around their local maxima and minima are merely graphical artefacts due to a finite sample of points.

$\epsilon_n(0, t) = \dot{u}_n(t)$ for $E = 0$, and with a curvature related to the derivative of the energy H of the solution $u_n(t)$ with respect to its frequency ω_b as [17]

$$\left.\frac{d^2E}{d\theta^2}\right|_{\theta=0} = -\frac{\omega_b^2}{\pi}\frac{dH}{d\omega_b}. \tag{A.2}$$

In figure A1(a) the breather is still localized, and the phase mode band is flat while the other bands, corresponding to extended phonon modes, are steep around $E = 0$. We note that as the phase mode band collides with the phonon mode bands, its trace can be followed as a 'ghost path' consisting of 'wiggles' on the phonon mode bands [27]. These wiggles connect each phonon mode band which corresponds to a mode with the same spatial symmetry as the breather to the neighbouring band of the same symmetry, while bands corresponding to modes of opposite symmetry are left unchanged. Thus, due to the presence of the breather, the bands corresponding to the spatially symmetric modes will not have a unique wave vector q as they would have in the absence of the central breather, but consist of different parts with different wave vectors connected to each other. In particular, the phase mode band is connected to the symmetric band edge ($q = \pi$) phonon mode constituting the band indexed '1' in figure A1.

Now, approaching the point where $2\omega_b$ enters the phonon band (figure A1(b)) the phonon mode bands move upwards, and the intersections with the axis $E = 0$ move closer to $\theta = 0$. Note however that due to the wiggled nature of the bands the closest intersection in fact belongs to the band indexed '3' and not to the band '1' which is connected to the phase mode, and approaching the point of resonance $\omega_b \approx 0.5745$ this intersection will appear on its flat part. Consequently, the intersection point will be 'repelled' from $\theta = 0$ at the point of resonance, yielding the avoided collision in figure 2(c). If the system size is increased there will be more bands and the distance between neighbouring bands decreases, and thus the flat part between two connected bands becomes shorter and the closest intersection point approaches $\theta = 0$ in the limit of an infinite system as illustrated in figure 2(d).

Comparing the band spectra just before and after the breather–phonobreather transition (figures A1(b) and (c)) we see no drastic changes, but rather a continuous deformation of the bands. In particular, we should note the gradual increase of curvature of the phase mode band, consistent according to (A.2) with the change of slope of the curve $H(\omega_b)$ in figure 4(d). We should also note the 'dip' of the band '3', which in the absence of a breather would have constituted the lower part of the band edge $q = \pi$ band, and whose minimum then would have crossed $E = 0$ exactly at the point of resonance yielding a true collision of Floquet eigenvalues at +1. Decreasing ω_b further into the pure phonobreather regime (figure A1(d)) the curvature of all bands becomes smaller and the 'dip' character of the lower part of band '3' disappears, corresponding to the regime where the Floquet eigenvalues move away from $\theta = 0$ in figures 2(b) and (c). Moreover, the bands move upwards, and in figure A1(e) the minimum of band '2', corresponding to spatially antisymmetric modes, cuts $E = 0$ yielding the instability at $\omega_b \approx 0.4711$ seen in figure 2(c). Finally, we show in figure A1(f) how eventually also the minimum of band '3' reaches $E = 0$, yielding the collision at +1 of Floquet eigenvalues at $\omega_b \approx 0.4346$ in figure 2(c) and an instability for smaller ω_b.

References

[1] Aubry S 1997 *Physica* D **103** 201–50
[2] Flach S and Willis C R 1998 *Phys. Rep.* **295** 181–264
[3] MacKay R S 2000 *Physica* A **288** 174–98
[4] Aubry S and Kopidakis G 2001 Aspects of discrete breathers and new directions *Nonlinearity and Disorder: Theory and Applications. Proc. NATO ARW (Tashkent, Uzbekistan, 2–6 Oct. 2000)* ed F Abdullaev *et al* (Dordrecht: Kluwer) pp 81–98 (*Preprint* cond-mat/0102162)
[5] MacKay R S and Aubry S 1994 *Nonlinearity* **7** 1623–43
[6] Flach S 1995 *Phys. Rev.* E **51** 1503–7
[7] Bambusi D 1996 *Nonlinearity* **9** 433–57
[8] Sepulchre J-A and MacKay R S 1997 *Nonlinearity* **10** 679–713
[9] Livi R, Spicci M and MacKay R S 1997 *Nonlinearity* **10** 1421–34
[10] Aubry S 1998 *Ann. Inst. H Poincaré Phys. Théor.* **68** 381–420

[11] Aubry S, Kopidakis G and Kadelburg V 2001 *Disc. Cont. Dyn. Syst.* -B **1** 271–98
[12] Baesens C and MacKay R S 1997 *Nonlinearity* **10** 931–40
[13] Marín J L and Aubry S 1996 *Nonlinearity* **9** 1501–28
[14] Flach S 1996 *Physica* D **91** 223–43
[15] Boyd J P 1990 *Nonlinearity* **3** 177–95
[16] Bonart D 1997 *Phys. Lett.* A **233** 233–8
[17] Kopidakis G and Aubry S 1999 *Physica* D **130** 155–86
[18] Kopidakis G and Aubry S 2000 *Phys. Rev. Lett.* **84** 3236–9
Kopidakis G and Aubry S 2000 *Physica* D **139** 247–75
[19] Morgante A M 2001 Multibreathers et ondes stationnaires dans des résaux discrets non-linéaires *PhD Thesis* Ecole polytechnique, Palaiseau, France (in French)
[20] Morgante A M, Johansson M, Kopidakis G and Aubry S 2000 *Phys. Rev. Lett.* **85** 550–3
[21] Morgante A M, Johansson M, Kopidakis G and Aubry S 2002 *Physica* D **162** 53–94
[22] Marín J L, Aubry S and Floría L M 1998 *Physica* D **113** 283–92
[23] Cretegny T 1998 Dynamique collective et localisation de l'énergie dans les résaux non-linéaires *PhD Thesis* Ecole normale supérieure, Lyon, France (in French)
[24] Speight J M and Sutcliffe P M 2001 *J. Phys. A: Math. Gen.* **34** 10839–58
[25] Yang J, Malomed B A, Kaup D J and Champneys A R 2001 *Math. Comput. Simul.* **56** 585–600
[26] Johansson M and Aubry S 2000 *Phys. Rev.* E **61** 5864–79
Johansson M 2001 *Phys. Rev.* E **63** 037601-1–4
[27] Marín J L and Aubry S 1998 *Physica* D **119** 163–74
[28] Kress J D, Saxena A, Bishop A R and Martin R L 1998 *Phys. Rev.* B **58** 6161–5
[29] Kopidakis G and Aubry S 2001 *Physica* B **296** 237–50
[30] Sukhorukov A A, Kivshar Yu S, Bang O and Soukoulis C M 2000 *Phys. Rev.* E **63** 016615-1–9